in the same manner as was used for the turbulent case. The results are analogous to those obtained in the turbulent case and are shown in the insert of Fig. 2.

Thus, a calculation of the zero angle-of-attack distribution together with a detailed surface pressure distribution should allow for a quick evaluation of the turbulent or laminar heat-transfer distribution at various circumferential locations over a blunt cone at various angles of attack. This has been demonstrated for two sets of data. The extension of this type of correlation to conditions other than that described herein has been indicated, but this must be verified experimentally.

References

[1] Widhopf, G. F., "Turbulent Heat Transfer Measurements on a Blunt Cone at Angle of Attack," TR-0059(S6816-66)-1, Feb. 1971, The Aerospace Corp., San Bernardino, Calif.

[2] Vaglio-Laurin, R., "Turbulent Heat Transfer on Blunt-Nosed Bodies in Two-Dimensional and General Three-Dimensional Hypersonic Flow," *Journal of the Aerospace Sciences*, Vol. 27, No. 1, Jan. 1960, pp. 27–36.

[3] Fay, J. A. and Riddell, F. R., "Theory of Stagnation Point Heat Transfer in Dissociated Air," *Journal of the Aeronautical Sciences*, Vol. 25, No. 2, Feb. 1958, pp. 73–85.

[4] Bushnell, D. M., Jones, R. A., and Huffman, J. K., "Heat Transfer and Pressure Distributions on Spherically Blunted 25° Half Angle Cone at Mach 8 and Angles of Attack up to 90°," TN-D-4792, Oct. 1968, NASA.

[5] Vaglio-Laurin, R., "Laminar Heat Transfer on Three-Dimensional Blunt Nosed Bodies in Hypersonic Flow," *American Rocket Society Journal*, Vol. 29, No. 2, Feb. 1959, pp. 123–129.

[6] Widhopf, G. F., "Heat Transfer Correlations for Blunt Cones at Angle of Attack," TR-0172(S2816-63)-1, July 1971, The Aerospace Corp., San Bernardino, Calif.

Measurements of Shock Wave Location in Hypersonic Nitrogen Flow

MERVIN E. HILLARD JR.,* WILLIAM D. HARVEY,† AND M. LAWRENCE EMORY‡

NASA Langley Research Center, Hampton, Va.

WHEN a high-energy electron beam interacts with a flowing gas, two sources of radiation may be used to visualize the flow structure: the fluorescence from direct excitation[1,2] and afterglow[3,4]; both sources have been used in flowing nitrogen gas media to study plumes and flow fields about simple configurations. This Note describes the technique of electron-beam flow visualization used in the Mach 19 Hypersonic Nitrogen Facility[5] for quantitative studies of complex, three-dimensional shock waves about a space-shuttle configuration.

The electron gun and drift tube assembly[6] were mounted on top of the tunnel at the centerline (Fig. 1a), and static and dynamic calibrations of the beam deflection circuit were made. Two 35 mm cameras positioned at the side and on top of the tunnel recorded the flow patterns at a tunnel stagnation pressure and temperature of 2.4×10^7 N/m^2 and 1.65×10^3 °K.

Received March 25, 1971; revision received July 6, 1971.

Index categories: Entry Vehicles and Landers; Supersonic and Hypersonic Flow.

* Aero-Space Technologist, Instrument Research Division, Gas Parameters Measurements Section.

† Aero-Space Technologist, Hypersonic Vehicles Division, Gas Dynamics Section. Member AIAA.

‡ Engineering Technician, Instrument Research Division, Gas Parameters Measurements Section.

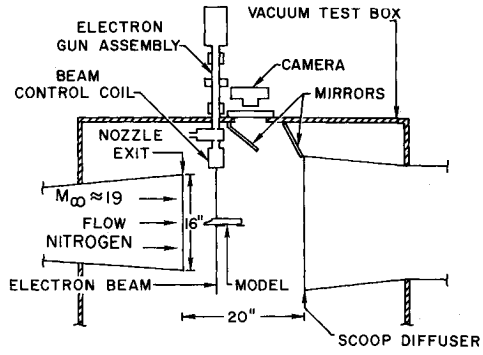

A) EXPERIMENTAL SETUP

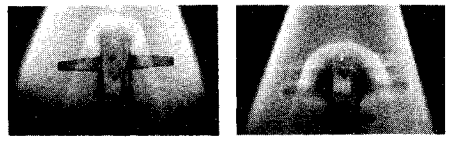

B) METHOD 1, α = 0°

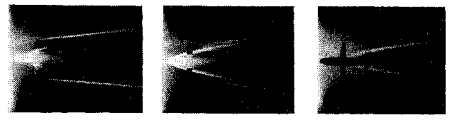

C) METHOD 2. α = 15°

Fig. 1 Experimental setup and typical sequences of two-dimensional cross sections through the shock structure.

Two methods were used to visualize the flow. First, the beam was swept in a plane perpendicular to the flow, and the position of this plane in the flow direction was varied in discrete steps; photographs, looking upstream at the model, were taken at each position of the beam plane (Fig. 1b). In this method the directly excited fluorescence produced in the plane of the beam enhanced the shock structure. Second, a collimated beam was stepped across the flow upstream of the model, and through the side window a photograph was taken at each step of the beam to show two-dimensional "slices" of the flow structure (Fig. 1c). The beam position calibration determined the location of each slice with respect to the model and the afterglow enhanced the flowfield.

In the initial quantitative tests, the flowfield about a sharp flat plate (0.13 m wide and 0.20 m long) at zero angle of attack was studied. The second method was used to map the flow structure about the flat plate, and for the data in this note, the beam was positioned to illuminate a slice through the shock layer along the center of the plate. Parameters calculated from measurements of the photographs included shock wave location (outer edge) y_s, boundary-layer thickness y_δ, and density ratio across the shock ρ_{max}/ρ_∞. (The effect on the data of varying film exposure was not investigated.) Figure 2a shows the shock wave location determined from the flow visualization photographs and, for comparison, two empirical calculations[7,8] and measurements of the shock location based on pitot pressure (P_{t_2}) data and schlieren photographs. (Details on construction and dimensions of pressure and temperature probes are available in Ref. 9.) The shock position from the pitot probe measurements was chosen as the location of the maximum in pressure (see insert, Fig. 2a). The flow visualization photographs also showed a bright region extending from the shock location to approximately one-half the distance from the shock to the plate; the edge of this bright region was interpreted as the edge of the boundary layer and the bright area as the higher density inviscid region. This presumed boundary-layer edge is compared with that obtained from the pitot pressure and total temperature (T_t)

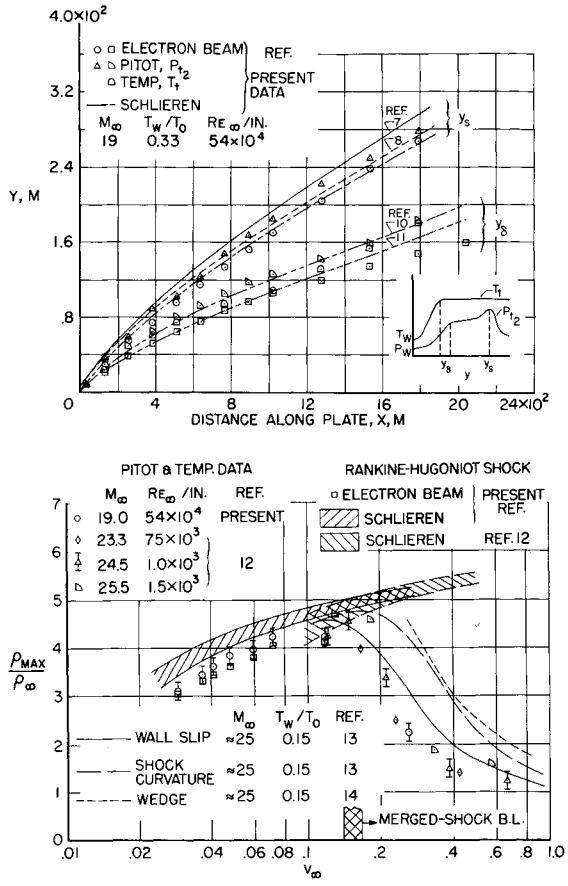

Fig. 2 Flowfield parameters for a sharp flat plate; a) shock shape and boundary-layer thickness, b) maximum density ratios across shock.

measurements and two empirical calculations.[10,11] Boundary-layer thicknesses from the probe measurements were chosen as the distance from the surface of the plate where a knee occurred in the profile data (see insert, Fig. 2a). Insufficient contrast occurred on the schlieren photograph to locate the boundary-layer edge. Figure 2 shows good agreement between the electron-beam measurements and the schlieren measurement for shock wave location, while the boundary-layer thickness follows the prediction according to Feldhuhn.[11]

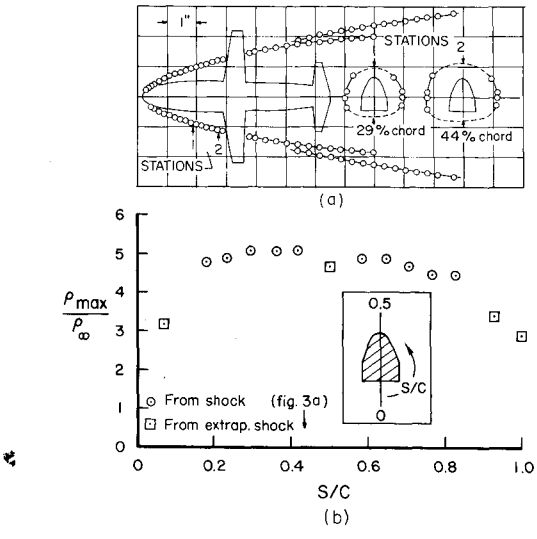

Fig. 3 Representative shock standoff and maximum density ratio across shock for space-shuttle configuration; a) planform and cross section, b) maximum density ratio at 36% chord.

Shown in Fig. 2b is a comparison between the present results and other experimental and theoretical results[12–14] for the density ratio across the shock as a function of the viscous interaction parameter, $\bar{V}_\infty$.[12] The electron beam density ratios were determined by measuring the shock angle from the photographs and calculating the density ratio from oblique shock relations. The results compare well with the density ratios calculated from the probe measurements both in magnitude and trend for $\bar{V}_\infty$ less than 0.12 and also agree with previous experimental[12] and theoretical[13] (wall slip) results for $\bar{V}_\infty$ less than 0.12.

The previously discussed agreement with other methods for obtaining values of y_s, y_δ, and ρ_{max}/ρ_o on two-dimensional shapes justified the quantitative study of more complex flow patterns, therefore a mockup of a space-shuttle configuration was tested (the model appears in Fig. 1). In these tests, the second method was used to produce a set of photographs similar to those in Fig. 1c. A plot of the coordinates of the shock from each photograph was made, and since the position of each slice was known, this sequence of plots formed a quantitative, three-dimensional map of the shock location about this space-shuttle model.

From this three-dimensional map, Fig. 3a shows a planform of the shock located along a mid-section of the model and two cross sections through the shock envelope located at stations 1 and 2. (The angles of attack and yaw were approximately 2° and 1°, respectively, and the free-stream Reynolds number based on model length was 32.4×10^4 and $M_\infty \simeq 19$.) The dashed lines indicate a possible extrapolation of the shock envelope since the data only showed that the shock envelope must lie within the arrows because in these tests the distance between each step in the movement of the electron beam was not sufficiently small to cover this area.

From Fig. 3a, the shock angle about a station located approximately halfway between stations 1 and 2 was determined by measuring the shock standoff distance along a line perpendicular to the surface of the model for several points around the model at stations 1 and 2. The change in shock position from station 1 to station 2 determined the shock angle. From this and the freestream Mach number M_∞, the density ratio across the shock was calculated. Figure 3b shows this density ratio for several points around the model for a station located at approximately 36% chord. (S designates surface distance around the model and C the model circumference.)

There are numerous modes of operation of the electron-beam system capable of displaying three-dimensional flowfields and shock shapes. The methods described proved useful for obtaining quantitative data on shock wave location, boundary-layer thickness, and density ratio across a shock in three dimensions for complex flow structures in the Langley Hypersonic Nitrogen Facility.

References

[1] Rothe, D. E., "Flow Visualization Using a Traversing Electron Beam," *AIAA Journal*, Vol. 3, No. 10, Oct. 1965, pp. 1945–1946.

[2] Maguire, B. L., Muntz, E. P., and Mallin, J. R., "Visualization Technique for Low-Density Flow Fields," *IEEE Transactions on Aerospace and Electronic Systems*, Vol. AES-3, No. 2, March 1967, pp. 321–326.

[3] Grun, A. E., Schopper, E., and Schumacher, B., "Electron Shadowgraph and Afterglow Pictures of Gas Jets at Low Densities," *Journal of Applied Physics*, Vol. 24, 1953, pp. 1527–1528.

[4] Sebacher, D. I., "Flow Visualization Using an Electron-Beam Afterglow in N_2 and Air," *AIAA Journal*, Vol. 4, No. 10, Oct. 1966, pp. 1858–1859.

[5] Clark, F. L., Ellison, J. C., and Johnson, C. B., "Recent Work in Flow Evaluation and Techniques of Operations for the Langley Hypersonic Nitrogen Facility," *Advanced Experimental Techniques for Study of Hypervelocity Flight*, Vol. 1, 1967, pp. 347–373.

[6] Hillard, M. E., Jr., Ocheltree, S. L., and Storey, R. W., "Spectroscopic Analysis of Electron-Beam Induced Fluorescence in Hypersonic Helium Flow," TN D-6005, Oct. 1970, NASA.

[7] Pan, Y. S. and Probstein, R. F., "Rarefield Flow Transition at a Leading Edge," Fluid Mechanics Lab. Rept. 64-8, 1964, MIT, Cambridge, Mass.

[8] Hays, W. D. and Probstein, R. F., *Hypersonic Flow Theory*, Academic Press, New York, 1959, pp. 275–389.

[9] Beckwith, I. E., Harvey, W. D., and Clark, F. L., "Comparisons of Turbulent Boundary-Layer Measurements at M = 19.5 with Theory and an Assessment of Probe Errors," TN D-6192, 1971, NASA.

[10] Bertram, M. H. and Feller, W. V., "A Simple Method for Determining Heat Transfer, Skin Friction, and Boundary-Layer Thickness for Hypersonic Laminar Boundary-Layer Flows in a Pressure Gradient," Memo 5-24-59L, 1959, NASA.

[11] Feldhuhn, R. H., "An Experimental Investigation of the Effects of Leading Edge Reynolds Number and Angle of Attack on the Flow of Helium Over a Flat Plate at M = 16.35," Internal Memo 8, July 1965, Princeton Univ., Princeton, N. J.

[12] McCroskey, W. J., "An Experimental Model for the Sharp Leading Edge Problem in Rarefield Hypersonic Flow," ARL 66-0101, June 1966, Aerospace Research Lab., Wright-Patterson Air Force Base, Ohio.

[13] Shorenstein, M. L. and Probrtein, R. F., "The Hypersonic Leading Edge Problem," AIAA Paper 68-4, New York, 1968.

[14] Rubin, S. G., Lin, T. C., Pierucci, M., and Rudman, S., "Hypersonic Interactions Near Sharp Leading Edges," PIBAL Rept. 68-17, June 1968, Polytechnic Inst. of Brooklyn, Brooklyn, N. Y.

Simplified Radiation Analysis Using Modularized Enclosures

JOHN J. CHAPTER* AND J. M. CONNOLLY†
Martin Marietta Corporation, Denver Division

Nomenclature

A_i	=	area of node i
F_{i-j}	=	over-all radiant interchange factor from i to j
i	=	ith node of enclosure or subenclosure
j	=	jth subenclosure
m,m'	=	*MESS* node located in subenclosure j and adjacent subenclosures, respectively
n	=	nth subenclosure
N	=	number of nodes in thermal network enclosure or subenclosure
P_i	=	number of primary radiators for node i
Q_i	=	total heat load for node i
r,r'	=	*MESS* node located in subenclosures n and j, respectively
R_n,R_j	=	number of *MESS* node interfaces in subenclosures n and j, respectively
T	=	absolute temperature
T_i,T_i'	=	exact and approximate temperature of ith node
γ	=	primary radiation fraction, radiators of a node left intact divided by the sum of the node radiators
σ	=	Stefan-Boltzmann constant

Subscripts

ERN	=	effective radiation steady-state node
h,k,l	=	enclosure, subenclosure nodes
MESS	=	multiple enclosure simplification shield

THE Radiation Condenser (RC) computer program[1] has been generalized to include a new technique of enclosure radiative analysis simplification referred to as the Multiple Enclosure Simplification Shield (*MESS*) technique.[2] The generalized RC computer program presented in this Note makes application of the *ERN/MESS* technique practical in the MITAS[3] thermal analyzer and provides a single tool for radiation analysis optimization. The program is presently being used on the NASA Skylab and Viking projects where computer run times have been reduced as much as 80%.

Received May 10, 1971; revision received June 18, 1971.
Index category: Thermal Modeling and Experimental Thermal Simulation, Radiation and Radiative Heat Transfer.

* Group Engineer, Skylab Apollo Telescope Mount Thermal Unit. Member AIAA.
† Engineer, Skylab Apollo Telescope Mount Thermal Unit. Member AIAA.

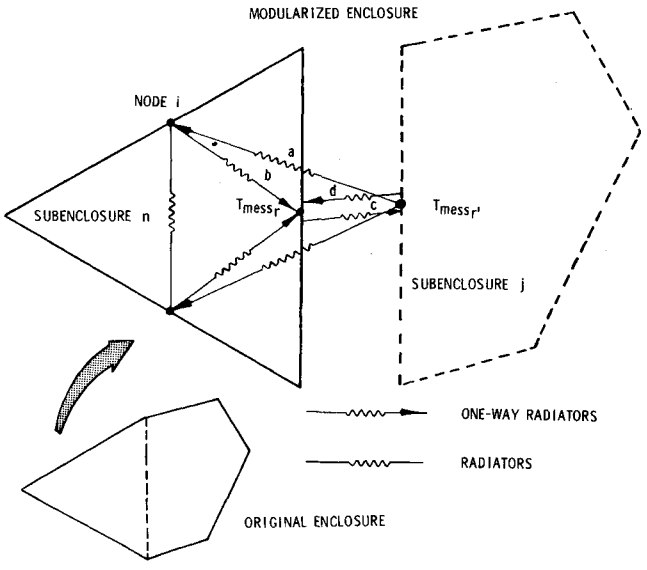

Fig. 1 *MESS* technique one-way radiators.

The *ERN* technique is used to reduce the number of radiative couplings (radiators) required to thermally model enclosures. *MESS* enables a complex enclosure to be modularized into discrete subenclosures by assigning imaginary interface shield nodes. The smaller enclosures can be analyzed efficiently with existing computers. Additionally, each subenclosure can be analyzed independently of the others which may result in more efficient use of manpower.

ERN/MESS Technique

The *ERN* and *MESS* techniques are independent and may be discussed separately. Consider an N node radiative enclosure that forms a section of a complex thermal network. The temperature of node i is a function of radiation, conduction, convection, and applied heat loads. Also assume that the contribution to the temperature of node i from the conduction and convection terms are included in the heat load Q_i. The steady-state temperature of node i is

$$T_i = \left[\left(\sum_{k=1}^{N} \sigma A_i F_{i-k} T_k^4 + Q_i\right) \Big/ \sum_{k=1}^{N} \sigma A_i F_{i-k}\right]^{1/4} \quad (1)$$

Application of the *ERN* technique requires that the radiators of node i be divided into P_i primary and $N - P_i$ secondary terms. Radiators for node i can then be written:

$$\sum_{k=1}^{N} \sigma A_i F_{i-k} T_k^4 = \sum_{k=1}^{Pi} \sigma A_i F_{i-k} T_k^4 + \sum_{l=P_{i+1}}^{N} \sigma A_i F_{i-l} T_l^4 \quad (2)$$

The number of radiators is reduced by replacing the secondary radiator summation with a single term coupled to an *ERN*. The temperature is calculated by the thermal analyzer program as a radiator-weighted steady-state temperature using secondary radiator sums.

$$T_{ERN} = \left[\sum_{i=1}^{N} \sum_{l=P_{i+1}}^{N} \sigma A_i F_{i-l} T_i^4 \Big/ \sum_{i=1}^{N} \sum_{l=P_{i+1}}^{N} \sigma A_i F_{i-l}\right]^{1/4} \quad (3)$$

Application of the *MESS* technique enables a radiative enclosure to be divided into an arbitrary number of subenclosures. *MESS* node pairs are defined by the analyst at the